e-J. Surf. Sci. Nanotech. Vol. 16 (2018) 163-171 Conference - ISSS-8 -

Structure and Reactivity of Cu-doped Au(111) Surfaces*

Federico Grillo,† Rory Megginson, Jenny Christie, Stephen M. Francis,
Neville V. Richardson, and Christopher J. Baddeley
EaStCHEM - School of Chemistry, University of St Andrews, St Andrews, KY169ST, United Kingdom
(Received 8 January 2018; Accepted 1 April 2018; Published 19 May 2018)

The structure and surface chemistry of ultrathin metallic films of one metal on another are strongly influenced by factors such as lattice mismatch and the formation of near-surface alloys. New morphologies may result with modified chemical properties which in turn open up different routes for molecular adsorption, desorption and surface functionalization, with important consequences in several fields of application.

The Cu/Au(111) system has received the attention of many studies, only a few however have been performed in ultra-high vacuum (UHV), using surface sensitive techniques. In this contribution, the room temperature deposition of copper onto the (22 $\sqrt{3}$)-Au(111) surface, from submonolayer to thick film, is investigated using scanning tunnelling microscopy (STM).

The onset of copper adsorption is seen to occur preferentially at alternate herringbone elbows, with a preference for *hcp* sites. With increasing coverage, copper-rich islands exhibit a reconstructed surface reminiscent of the clean Au(111) herringbone reconstruction. Disordered, pseudo-ordered and ordered surface layers are observed upon annealing. Models for the initial adsorption/incorporation mechanism, formation of adlayers and evolution with increasing coverage and annealing are qualitatively discussed. Further, the reactivity of copper-doped Au(111) systems is considered towards the adsorption of organic molecules of interest in nanotechnology and in catalytic applications. [DOI: 10.1380/ejssnt.2018.163]

Keywords: Scanning tunneling microscopy; Cu; Au(111); Surface alloy

I. INTRODUCTION

The investigation of heteroepitaxial thin films can reveal important information related to films of novel compositions, the properties of which can be modified by a mutual substrate/adsorbate influence, giving rise to new systems with peculiar characteristics, making them of wide interest in several technological fields. In fact, ultrathin films of metals on single crystal metal surfaces can provide structurally interesting systems in which a delicate balance of forces arises from the lattice mismatch of the overlayer and the substrate. Because of this mismatch, surface layers are generally stressed and tend to minimize the excess energy by means of surface reconstruction [1–3]. Heteroepitaxial metallic systems are relevant in different fields, such as elucidating metal-on-metal growth and describing phenomena occurring at metal/metal interfaces. They can also be exploited in the formation of networks based on monodispersed, regularly spaced, features and in heterogeneous catalysis when a crucial control of the spatial distribution of two metallic centers is required.

Among the fcc metals, the Au(111) surface offers a unique substrate for heteroepitaxy because of its peculiar characteristic to reconstruct even at room temperature exhibiting a (22 $\sqrt{3}$) superstructure, the so-called herringbone reconstruction [4], generated by a unidirectional compression along $\langle 1\bar{1}0 \rangle$ equivalent directions of the top layer, accommodating 23 top layer gold atoms in 22 bulk lattice atomic spaces. In the top layer this introduces stress points and very reactive sites (the elbows) where the majority of adsorbed metals are seen to condense preferentially. Nucleation of guest metals on Au(111) generally occurs via the place-exchange mechanism [5], which was initially ruled out for the adsorption of copper; however, it was later reported that the onset of copper adsorption does occur via a place-exchange mechanism, at specific sites identified as the narrowed regions within the highly reactive elbows of the Au(111)-(22 $\sqrt{3}$), irrespective of hcp or fcc stacking [1]. Other than for copper [6–8], this is also the case for other transition metals such as nickel [9–12], iron [13, 14], and chromium [15, 16], to name a few. Added clusters are regarded as a source of reactive metal atoms, over a surface commonly considered as a 2D inert support, opening up the possibility of modifying the reactivity of the Au(111) surface itself, via the formation of surface alloys, whereby both the added metal and gold are present in the top layer.

In this contribution the structures of Cu-doped Au(111) surfaces, prepared under ultra-high vacuum (UHV) conditions, are illustrated and discussed, in relation to copper loading, from just a few atoms to thick copper layers, and annealing treatments. Some examples of reactivity of Au(111) surfaces modified with the addition of copper, towards the adsorption of molecular adsorbates, are given. Finally, some of the future challenges and open questions are highlighted.

II. EXPERIMENTAL

Measurements were undertaken on an Omicron variable temperature STM, operated at room temperature, in an ultra-high vacuum environment with a base pressure of about 1 10^{-10} mbar or lower. STM images were acquired at room temperature in constant current mode using electrochemically etched tungsten tips. The tunneling voltage bias was applied to the tip, whereas the sample was grounded. Images were processed with the WSxM software package [17]. Images are not corrected for thermal drift. Copper was deposited on the Au(111) crystal kept at room temperature by electrically heating a high

This paper was presented at the 8th International Symposium on Surface Science, Tsukuba International Congress Center, Tsukuba, Japan, October 22-26, 2017.
† Corresponding author: federico.grillo@st-andrews.ac.uk

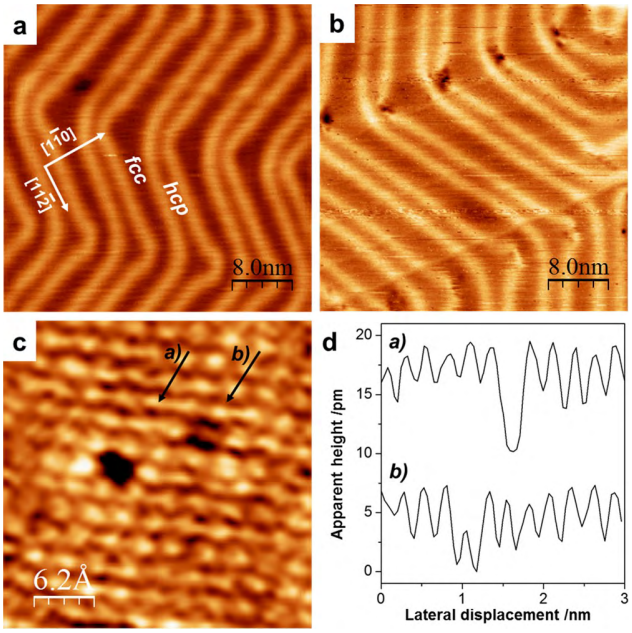

FIG. 1. STM images showing (a) clean Au(111); (b) after dosing less than ca. 0.01 ML Cu on Au(111); (c) atomic resolution after less than ca. 0.01 ML Cu on Au(111) and (d) corresponding line profiles highlighting a) an Au vacancy and b) an Au vacancy filled by a Cu atom. (a) 40 40 nm^2, 1:0 V, 0.5 nA; (b) 40 40 nm^2, 1:0 V, 0.8 nA; (c) 3:1 3:1 nm^2, 0:5 V, 0.2 nA.

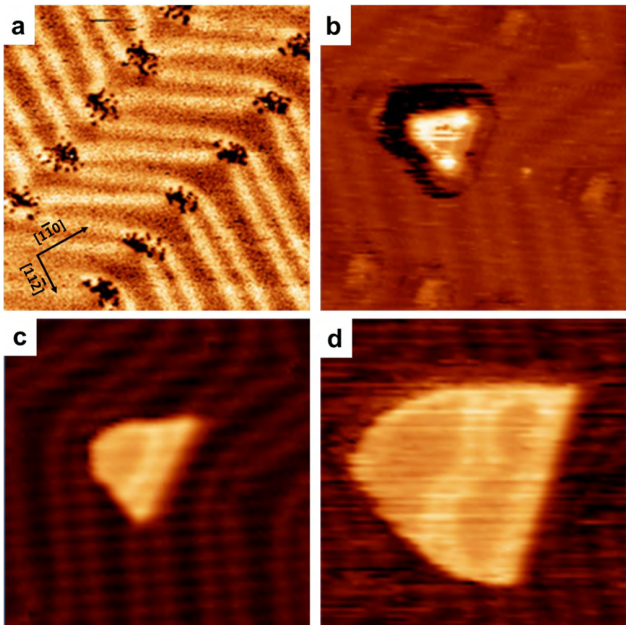

FIG. 2. STM images showing the evolution of Cu rich island with increasing Cu coverage (see text for details on coverage evaluation [1]; the local coverage shown on these individual zoomed-in images is higher than the overall coverage evaluated on the respective full size images). (a) ca. 0.025 ML Cu, 40 40 nm^2, 1:0 V, 0.78 nA; (b) ca. 0.025 ML Cu, 35 35 nm^2, 1:28 V, 1.1 nA; (c) ca. 0.062 ML Cu, 28 28 nm^2, 1:25 V, 0.76 nA and (d) ca. 0.18 ML Cu, 32 32 nm^2, 1:2 V, 0.84 nA.

purity copper wire (99.999%, 0.1 mm diameter), wrapped around a tantalum wire (99.999% purity, 0.25 mm diameter), to yield a deposition rate of ca. 0.07 ML min^{-1}. The local coverage was determined by evaluation of surface topographical features observed on the STM images. The overall nominal coverage in monolayer (ML) was determined by evaluating the fraction of each image covered by the features related to copper and their appearance, in combination with the calculated exposure. In the assumption of epitaxial growth, with no intermixing, a 1 ML coverage is defined as one copper atom per surface unit cell of Au(111).

The Au(111) crystal was cleaned by cycles of argon ion sputtering and annealing to ca. 870 K until wide terraces characterized by the typical Au(111)-(22 $\sqrt{3}$) surface reconstruction were observed on STM.

III. RESULTS AND DISCUSSION

A. Structure

1. *Low coverage regime (up to ca. 1 ML).*

Figure 1 shows STM images of the clean Au(111) surface [Fig. 1(a)] and following copper deposition up to a coverage of ca. 0.01 ML [Fig. 1(b)], at room temperature. Dark features [1], ascribed to the presence of copper, appear between every pair of ridges that create a narrowed elbow, with a preference for hcp sites. Copper nucleation is thought to occur via the place-exchange mechanism proposed by Meyer and co-workers and initially thought unfavourable [5]: one copper atom replaces one gold atom in the first layer and the replaced gold atoms undergo rapid diffusion over the terrace eventually condensing at a nearby step edge. This is a dynamic process revealed by the fuzzy appearance of the STM images during scanning and of the gold step edges [1].

Figure 1(c) presents an atomically resolved STM image in which both an ejected gold atom, a gold vacancy, along profile a) and a nearby gold atom substituted by a copper atom can be seen, along profile b); line profiles are shown in Fig. 1(d). Recently, dark features were attributed to embedded copper atoms, rather than to missing gold atoms [18]. The dark appearance of the copper atoms is tentatively explained on the basis of both electronic and geometrical considerations. Copper and gold are characterised by different work functions, 4.93 eV for Cu(111) [19] and 5.35 eV for Au(111) [20]. This work function difference will result in a local redistribution of electron density and a charge compensating electron transfer is likely to occur resulting in a small net charge flow from copper to gold [21–23]. A similar interpretation was given to explain the dark appearance of copper atoms deposited on Pt(111) [24]. Nevertheless, electronic considerations alone may not be sufficient to explain this observation as it was also observed [25] for systems in which work functions values for the guest (gold) and the host (Ni(111), 5.35 eV [26]) are very similar. A contribution to the copper contrast derives from geometrical factors: DFT calculations show that a copper atom incorporated within the first gold layer not only appears smaller than gold, but also has a tendency to sink towards the second gold layer [1].

Figure 2 shows the evolution of copper-rich islands with

increasing coverage. At increased coverage, 0.025 ML, Fig. 2(a), copper condensation is found in both fcc and hcp stacking regions. This indicates that the most favoured location for copper nucleation is in the vicinity of those gold atoms where the change in bridge site orientation occurs [1], even though at the atomic level the place exchange mechanism is favoured on hcp sites. Upon further addition of copper, Fig. 2(b), all the original condensation sites expand; their appearance changes from dark features to brighter, circular ones. This is interpreted as on-top copper growth, whereby further copper atoms condense on the initial nucleation sites. This may explain why the copper coverage as determined from STM images stays approximately constant, ca. 0.025 ML, even though nearly a double amount of copper was dosed. At this stage copper-rich regions are still confined within the narrowed regions at the herringbone reconstruction elbows regardless of the underlying gold stacking.

On-top copper growth is in agreement with the values for the cohesive energy for copper (about 3.53 eV) and for gold (about 3.78 eV) [2, 27], indicating that the condensation of copper on copper is slightly less expensive than the condensation of copper on gold. With increasing coverage, copper islands appear to enlarge and evolve into 'D'-shaped features [Fig. 2(c), ca. 0.062 ML] characterized by discommensuration lines reminiscent of the $(22 \sqrt{3})$ reconstruction, albeit more disordered [1]. Such surface corrugation was previously observed experimentally [28, 29] and was attributed to areas of accumulated stress in computational studies [30, 31].

Due to the inequivalence between hcp and fcc sites, with the former more favorable, islands initiated at hcp elbows increase in size, at the expense of those nucleated on fcc elbows sites via a mechanism consistent with an Ostwald ripening process, until they merge into very few, to the extent that from about 0.5–0.6 ML the surface top layer shows large copper-rich areas next to bare gold ones [1, 32, 33].

Copper-rich islands have an apparent height of ca. 0.175 nm [1, 34], a value much shorter than that expected for Cu–Cu (0.208 nm) and Au–Au (0.236 nm) monatomic steps on the respective f 111g planes. Considering these step height measurements and since nucleation occurs via a place-exchange mechanism, with copper atoms embedded within the first gold layer appearing as depressions, which then evolve into islands appearing as protrusions, copper-rich islands are thought to be two atomic layers thick, the first one of which is incorporated into the gold surface layer.

The composition of the top layer of thin metal films on metal surfaces has often been a matter of debate, because of intermixing phenomena. Copper and gold are known to be miscible already from room temperature [3], can form binary solid solutions across the full compositional range, and can also form ordered alloys in the bulk phase, most notably Cu_3Au, CuAu and $CuAu_3$. For the copper-gold system different top layer structures have been proposed: segregation [7, 30, 35, 36], complete encapsulation, whereby a single layer of copper is covered by a single layer of gold [32, 36–38] and intermixing [28, 32, 36–40] have been considered. Often varying electronic contrast observed via STM when imaging an island has been considered as an indication that the top layer is of mixed (random) composition, as in surface solid solution [12, 32, 41–43]. In the present case, as already highlighted, considering the growth behavior and the almost uniform contrast across an island [44], albeit increased in correspondence of the corrugation, the preference goes for an almost pure copper double layer, the first of which is incorporated within the top gold layer [1]. In fact, intermixing between the two metals cannot be totally ruled out, as atomically resolved STM images seem to show a random distribution of atoms with varying contrast which suggest attribution to the two metal atoms [32, 43].

A second layer exhibiting copper related features is seen to grow before the first one is completed.

2. High coverage regime (from above ca. 1 ML to ca. 20 ML).

Figure 3 shows structures formed after preparation and upon annealing a surface showing features attributed to up to three copper related layers. After preparation, the surface exhibits different reconstructions, depending upon the number of copper layers grown [Fig. 3(a)]: i) indicates an area of almost bare gold; some copper is likely to be present, as the herringbone reconstruction seems a little distorted; ii) the first copper (rich) layer, which reconstructs in a manner similar to the herringbone; iii) and iv) second and third copper layers, characterized by moiré patterns due to the interference between the Cu(111) and Au(111) lattices. The appearance of a moiré pattern may be considered as an indication that only a small amount of intermixing between the two metals can occur. On the basis of dI /dV measurements, at a coverage thicker than ca. 3 copper related layers the system behaves as a bulk copper f 111g terminated, as the field emission resonances due to Gundlach's oscillations remained almost unchanged at 4.7 eV [32], value in good agreement with that of the Cu(111) work function. Height profile measurements confirm a step height of ca. 0.175 pm for the first copper-rich layer, as previously observed [1, 34], and shows a step height of ca. 220 pm for the following layers [32], Fig. 3(d), profile a). Figure 3(b) shows a magnification of the moiré pattern, which has an average pseudo-periodicity of ca. 4.46 nm and a corrugation of ca. 20 pm [see line profile b) in Fig. 3(d)]. After annealing to ca. 520 K, surface features evolve into a different moiré structure having much larger average pseudo-periodicity, ca. 10.58 nm [Fig. 3(c) and line profile c) in Fig. 3(d)]. The centers of the moiré interference spots are connected through bright topographical features similar to those observed for the low coverage regime. These features consist of single and double ridges, having a corrugation of ca. 0.02 nm, over a varying contrast background, as better highlighted in the inset, which shows atomic resolution. This contrast variation qualitatively appears much more pronounced than for the initial growth (see Fig. 2 for comparison), and may indicate that a much higher amount of intermixing between the two metals can occur upon annealing. A similar moiré structure, with a relatively large periodicity, was observed following deposition of palladium on Au(111) [45]. Following an analogous data analysis, average spacings of ca. 0.280 nm and ca. 0.270 nm are calculated for the copper atoms, corresponding to expan-

FIG. 3. (a) STM images showing an area where up to 3 Cu related layers have been deposited, 150 150 nm^2, 1:0 V, 0.6 nA; (b) magnification of the moiré pattern over the 2nd and 3rd Cu related layers, 70 70 nm^2, 1:1 V, 0.8 nA; (c) after annealing to ca. 520 K, 70 70 nm^2, 1.1 V, 0.6 nA; in the inset atomic resolution, 25 25 nm^2, 1.1 V, 0.8 nA; (d) line profiles as in: a) Fig. 3(a); b) Fig. 3(b) and c) Fig. 3(c); (e) atomic resolution on the darker areas of Fig. 3(c), 2:6 2:6 nm^2, 0.6 V, 0.5 nA; (f) line profiles as in Fig. 3(e).

FIG. 4. STM images showing the evolution of structural features upon annealing a ca. 20 ML equivalent Cu film on Au(111); (a) as prepared, 250 250 nm^2, 0:8 V, 1.0 nA; (b) annealed to 370 K, 250 250 nm^2, 1:0 V, 1.4 nA; (c) annealed to 470 K, 250 250 nm^2, 1:0 V, 1.4 nA; (d) annealed to 570 K, 250 250 nm^2, 1:0 V, 1.0 nA; (e) annealed to 670 K, 250 250 nm^2, 1:0 V, 0.6 nA; (f) annealed to 750 K, 250 250 nm^2, 1:5 V, 1.77 nA; inset 40 40 nm^2, 1:3 V, 1.3 nA; (g) annealed to 800 K, 125 125 nm^2, 1:2 V, 0.98 nA; (h) line profiles as in Fig. 4(a–f).

sions of the ideal Cu(111) lattice of ca. 9.4% and ca. 5.4%, for the as prepared surface [Fig. 3(b)] and after annealing [Fig. 3(c)] respectively.

When atomic resolution is achieved upon the darker, flatter areas [Fig. 3(e)] two types of electronic contrasts can be clearly discriminated. The two electronic contrasts are attributed to gold, brighter, and copper atoms, dimmer, respectively and the lattice vectors are measured as ca. 0.27 nm and 0.53 nm, as shown by the line profiles a) and b) in Fig. 3(f). Atomic contrast and line profiles measurements indicate that the surface layer is represented by the CuAu alloy (type $L1_0$) as emerges also by comparison with the DFT calculations of Zhao and coworkers [37, 38]. Some theoretical studies have addressed the alloying behaviour of bulk Cu/Au systems. Of all possible structures, the most stable low temperature phase is in fact represented by CuAu (type $L1_0$), followed by Cu_3Au (type $L1_2$); $CuAu_3$ (again of $L1_2$ type), although ordered, is the least favourable [3, 46, 47].

Upon further annealing a pristine (22 $\bar{3}$) reconstruction reappears, implying that all the copper atoms have sunk deep into the bulk gold.

Figure 4 shows the appearance of the features produced upon deposition of copper to yield multilayer thick films. In Fig. 4(a), an amount of copper equivalent to ca. 20 layers is shown. Copper is seen to form pillars of hexagonal

shape with flat top surfaces. Annealing to progressively higher temperatures promotes dissolution of copper into the bulk gold. Qualitatively, the pillars appear to shorten and the surfaces of their top layers widen [Fig. 4(b–c)]. After annealing to 570 K, copper pillars merge and numerous screw dislocations appear over a non-uniform background. The darker areas in Fig. 4(d) exhibit a moiré structure, indicating that the copper layer is sufficiently thin that its lattice can interfere with the gold one [Fig. 4(d), white arrow]. The remaining surface shows a reconstruction similar to that in Fig. 3(c), which is taken as an indication of the formation of random intermixing between the two metals [12, 32]. Upon further annealing screw dislocations decrease in number and the contrast of the top layer becomes more homogeneous [Fig. 4(e), 670 K]. Eventually a pattern that can be attributed to an ordered surface alloy forms [750 K, Fig. 4(f) and inset]. Such a pattern is interpreted as alternating elongated domains of (almost) pure copper and (almost) pure gold, which recall the CuAu II alloy phase [46–48], characterized by periodic antiphase boundaries approximately every five unit cells along its y axis [48, 49]. The antiphase boundaries may be what is highlighted by the contrast change in the STM image in the inset of Fig. 4(f). The bulk AuCu phase diagram [46] shows that, for a 50 : 50 compositional ratio, the AuCu II is the prevalent stable phase, orthorhombic, yet incommensurate [49], and can be obtained by annealing at a very slightly higher temperature necessary to produce the tetragonal AuCu I phase. However, the AuCu I can be obtained by annealing to ca. 520 K, an initial nominal copper coverage of ca. 3 layers equivalent, as shown in Fig. 3. Interestingly interdiffusion of gold and copper may also result in the formation of the AuCu I phase, along with other disordered phases, as reported in some TEM studies [47, 50].

Step heights are measured as ca. 0.22 nm or multiples thereof, as shown in Fig. 4(h). The measured step height is a little higher than that of Cu (0.208 nm) and shorter than that of Au (0.236 nm) respective step heights f111g planes, but is taller than the Au-Cu(rich) step for submonolayer deposits, measured as ca. 0.175 nm. As highlighted, a reduced step height can be understood/rationalized both in terms of geometry as partial incorporation of copper into the gold layer and smaller radius for the copper atom, and local work function differences. In Ref. [32], a step height of 0.22 nm was measured for a 1L-Cu 2L-Cu step and was considered to be consistent with the step height of clean Cu(111). On the other hand, bulk Cu-Au alloys form solid solutions whose lattice parameters positively deviate from Vegard's law [51]. The lattice parameter is also shown to be representative of the bulk composition [51], to some degree of approximation. In the extreme assumption that a surface obtained by cleaving along f111g planes is representative of the bulk, knowing the crystal structure, the step height can give an estimation of the alloy composition. In this case, the measured value of 0.22 nm, well agrees with a Cu-rich alloy. Exceptions have to be made for the submonolayer deposits, when both electronic and geometrical factors may play a role in the measurement of the step height via STM, as already highlighted [1], and for the as prepared thick layers, when the step height is expected to approximate that of Cu(111).

A defect-free herringbone reconstruction reappears after annealing to ca. 800 K, as shown in Fig. 4(g).

B. Reactivity

To date, the primary use of bulk Cu-Au alloys, alone or with the addition of other precious metals, is in the production of jewelry; the relative ratio of the two metals is fine tuned in order to achieve a specific color and mechanical properties [48]. When considering metal surfaces, as already highlighted, added metal clusters on Au(111) are regarded essentially as a source of reactive metal atoms over a substrate commonly considered as a 2D inert support. For example, when copper doped Au(111) surfaces are dosed with organic molecules, this enables the study of copper coordinated metal-organic compounds. However, the adsorption of adsorbates might also induce morphological changes in the Cu/Au(111) system. For instance it can lead to chemically induced segregation [38, 52, 53]. In turn this renders processes like chemical titration unreliable methods for the determination of the surface composition, as strongly interacting titrants may extract the incorporated copper from the first/second gold layer. Out of the many available, some studies focusing on molecular adsorption on copper doped Au(111) surfaces, highlighting how added copper atoms can modify the adsorption behavior of the adlayers, are reported below.

Different metal-organic architectures can be prepared exploiting the reaction between carboxylic acid groups and copper. Tris-p-carboxylicpolychlorotriphenylmethyl radical (PTMTC) is a perchlorinated trityl radical derivative with an open shell electronic configuration stable and persistent at ambient conditions [54], with the unpaired electron mostly localized in the central carbon atom, C^* [8]. As revealed by combined STM and vibrational spectroscopy measurements, the balance between the affinity of chlorine atoms for gold [55] and the formation of hydrogen bonds, typical of carboxylic groups, steers molecular assembly to a flat-lying geometry on Au(111), whereby PTMTC radicals are characterized by intermolecular hydrogen bonding and interact with the gold surface through the chlorine atoms [56]. On copper doped Au(111) surfaces PTMTC was found to adopt an upright geometry [8], as a result of the deprotonation of one of the carboxylic acid groups followed by coordination with copper adatoms, and repulsive interaction between the Cl-substituted benzene rings. The change in geometry has important consequences regarding the preservation of the unpaired electron, as highlighted when comparing the calculated spin-projected density of states (SP-DOS) of the gas-phase free radical with those of the adsorbed species (Fig. 5). For the free radical, the spin-up and spin-down curves are asymmetric and a SOMO (Singly Occupied Molecular Orbital) state is present at 0:49 eV [Fig. 5(a)]. When adsorption occurs on Au(111), in the flat-lying geometry [Fig. 5(b)], the excess spin is lost, as evidenced by the totally symmetrical shape of the curves, whereas in the upright geometry on Cu/Au(111), the radical character is almost totally preserved [Fig. 5(c)] [8]. However, a more thorough characterization of the flat-lying species, especially of those in contact with the substrate, is still required, in

FIG. 5. Central C atom, C , SP-DOS diagrams for (a) a free PTMTC molecule, (b) PTMTC flat-lying on Au(111) and (c) coordinated with Cu and in an upright adsorption geometry on Cu/Au(111); black curves: spin up component; red curves: spin down component [8].

order to determine unambiguously whether the open shell structure is retained [8, 56, 57], and characterize the spin polarization [8, 56].

Different metal-organic species can be obtained through the use of N-containing compounds. Melamine has been shown to physisorb forming self-assembled hydrogen bonded structures on Au(111) [58], and to chemisorb upright on Cu(111) [59]. On Cu/Au(111) surfaces the adsorption behavior of melamine has been shown to change from flat-lying physisorption to upright chemisorption, manifesting an increased melamine-substrate interaction, at increasing copper film thicknesses [32]. This behavior, along with atomically resolved STM images, was taken as an indication that the copper and gold layers are defective and intermixed. When copper is evaporated on a melamine self-assembled monolayer (SAM) on Au(111), incorporation under the amine groups of melamine is reported [18]. The Cu–melamine interaction is regarded as moderate, as melamine doesn't appear to favour the segregation of copper atoms from subsurface to the top surface layer, yet sufficiently strong to disrupt locally the ordering of the hydrogen bonded supramolecular assembly. Such metal-organic structure has suggested to potentially act as a reservoir for supplying reactive atoms, if the chemistry of the system is tuned appropriately [18].

The coordination assembly of 1,3,5-trispyridylbenzene on Cu/Au(111) surfaces is reported to lead to a two-dimensional (2D) metal–organic honeycomb network, resulting from the coordination of copper with pyridyl (py) groups. These networks show great structural flexibility as several phases of different geometry and/or coordination appeared upon varying the coverage in organic linker (and hence the stoichiometric ratio with copper, and the surface density) [7].

Further, in a study considering porphyrins containing both pyridyl and Br-phenyl end groups [6], copper atoms deposited on Au(111) were not only exploited as metal centers in the formation of py–Cu-py metal–organic chains reacting with their pyridyl termini, but also suggested to play a role as a catalyst for the on surface Ullmann coupling reactions involving their Br-phenyl termini to form C–C covalent bonds.

FIG. 6. STM images of BTAH dosed to yield saturation on (a) Au(111), 15 15 nm^2, 1.04 V, 0.1 nA, acquired at 77 K; in the inset a not to scale model of the H-bonded motif [63]; (b) Cu(111), 14:5 14:5 nm^2, 0.69 V, 0.24 nA; in the inset a not to scale model of the basic unit made of three upright $Cu(BTA)_2$ and two upright CuBTA species [65]; (c) ca. 0.2 ML Cu/Au(111); a) indicates a Cu-rich island; b) indicates a Cu-decorated Au(111) herringbone elbow, 70 70 nm^2, 1:5 V, 0.7 nA; (d) close-up on herringbone reconstruction elbows, b) in panel (c); the dashed lines highlight the position of the herringbone reconstruction ridges; 20 20 nm^2, 1:0 V, 0.1 nA; (e) HREEL spectra (primary energy 4 eV, specular geometry, 5 meV resolution in the straight through geometry) collected for BTAH dosed to yield saturation on Au(111), black; Cu(111), blue; ca. 0.2 ML Cu/Au(111), as prepared, red; ca. 0.2 ML Cu/Au(111), after annealing to 320 K, dark red.

Benzotriazole (BTAH), amongst other uses, finds application as a corrosion inhibitor for copper and copper-containing objects, especially in water or humid environments. Its action is attributed to the formation of a water insoluble layer the structure of which is thought to comprise a metal-organic compound the structure of which is still a matter of debate [60–62]. By comparing BTAH

reactivity on different substrates, different interaction between BTAH molecules can be highlighted. STM measurements [Fig. 6(a), model in the inset] have shown that on Au(111) the chemistry of BTAH is characterized by weakly physisorbed flat-lying hydrogen bonded species, as also evidenced by the strong signals at 92 meV attributed to the CH out of plane bend mode, (C–H), and the absence of a CH stretch, (C–H), expected at ca. 380 meV in the HREEL (high resolution electron energy loss) spectrum [Fig. 6(e), black spectrum] [63]. On Cu(111) [64, 65] BTAH forms essentially densely packed layers comprised of BTA–Cu–BTA dimeric and CuBTA monomeric species, as shown by STM [Fig. 6(b); a model of the motif's basic unit is shown in the inset], chemisorbing in an almost upright configuration, with the triazole end toward the surface, as revealed by the decrease in intensity of the (C–H) mode, the presence of extra vibrations in the 100–200 meV range and the appearance of a strong (C–H) mode at ca. 378 meV [Fig. 6(e), blue spectrum]. TPD (temperature programmed desorption) experiments performed on Cu(111) have shown that desorption of physisorbed species occurs at ca. 400 K, whereas the chemisorbed dimer desorbs at ca. 595 K [65]. On Cu(110) flat-lying molecules in a (4 4) configuration [66, 67] are seen to coexist with the upright dimer [67]. A further insight into the BTAH–Cu interaction can be obtained via investigating BTAH adsorption on the Cu/Au(111) system. Upon BTAH deposition on a Au(111) surface dosed with ca. 0.2 ML of copper, STM shows fuzzy images due to fast diffusing adsorbates, as for adsorption on clean Au(111), and HREELS indicates flat-lying adsorption, as evidenced by the red spectrum in Fig. 6(e), which shows essentially the same modes as the spectrum collected of Au(111) [Fig. 6(e), black], albeit with a reduced intensity. Upon gentle anneal (ca. 320 K), in order to promote desorption of the weakly bound and diffusing species, BTAH is seen to coordinate with copper only in correspondence of copper-rich areas, at copper-rich island [a) in Fig. 6(c)] and copper decorated herringbone elbows [b) in Fig. 6(c)] and form monomeric, dimeric and perhaps polymeric species in an ensemble of different orientations, as shown by the dark red spectrum in Fig. 6(e), where modes attributed to flat-lying species mix with those generated by species whose molecular planes are at an angle with respect to the surface [68]. In particular, the $Cu_x(BTA)_y$ complex appears disordered when condensing over Cu-rich islands, but forming ordered structures when condensing at Cu-decorated herringbone elbows [Fig. 6(d)], where the brighter and almost parallel features might indicate upright adsorption, whereas the dimmer ones may account for species whose molecular plane is more parallel to the surface.

The effects of the adsorption of the amino acid glycine on Cu/Au(111) systems were considered by Zhao and coworkers, who concluded that at submonolayer coverage the two metals formed a surface alloy, whereas for copper coverages above the one monolayer, glycine adsorption causes the copper in the subsurface region to segregate to the substrate top layer [38].

Considering the adsorption of SO_2 on Cu/Au(111) surfaces, for copper coverages up to 1 ML, Zhao and coworkers reported a behavior different from pure copper and pure gold [37]. In particular, increased intermixing, accompanied by SO_2 desorption, as active sites necessary for SO_2 dissociation were determined not to be available, was observed upon annealing. The lack of such sites was regarded as an inherent feature affecting the prevention of alloys corrosion effects due to SO_2.

Okada and co-workers focused on oxygen induced corrosive phenomena on commercially available Cu_3Au(111), CuAu(111) and Au_3Cu(111) surfaces [69]. It was observed that systems with higher concentrations of gold in the top layer are less prone to oxidation. Oxygen adsorption induces segregation phenomena, the degree of which strongly depends on the bulk Cu_x/Au_y composition: the richer the gold bulk components, the richer the gold surface segregation. Au-rich layers are suggested to be able to form a protective layer against oxidation of the Cu-Au alloys; in particular, doping the external layers of copper-based materials with gold may work as an efficient protection against the oxidation of the surface and the near bulk regions.

From the catalytic point of view, supported copper and supported gold nanoparticles are very active for oxidation reaction and Cu/Au nanoparticulates have been reported to be catalytically active for a variety of reactions, in particular for the oxidation of CO and of alcohols to produce biofuels [70–72]. Moreover, supported gold catalytic systems can also operate as highly selective catalysts for the hydrogenation of important feedstocks such as benzaldehyde [73] and nitrobenzene [74]. An impediment to the use of gold for this type of catalytic chemistry is the high activation barrier for H_2 dissociative adsorption which limits the rate of hydrogenation and necessitates the use of undesirably high H_2 pressures. Alloying with other metals such as nickel and palladium have been shown to enhance hydrogenation rates [75, 76]. A recent report of supported copper catalysts being used to hydrogenate nitrobenzene using hydrogen supplied by the simultaneous dehydrogenation of 2-butanol [77], points to the possibility of using bimetallic Cu/Au catalysts to carry out similar coupled reactions exploiting the activity of copper for dehydrogenation chemistry and the very high selectivity of gold for a number of important hydrogenation reactions. A key advantage of the use of coupled reactions of this type is that there is no requirement for gas phase H_2 [77]. Our unpublished model studies on Cu/Au(111) surfaces have demonstrated an ability to tailor bimetallic active sites on Cu/Au surfaces. Further model studies will probe how the surface chemistry of relevant catalytic reactants is influenced by surface composition and the nature of bimetallic Cu/Au sites.

IV. CONCLUSIONS AND OUTLOOK

In conclusion, in this paper an STM study on the room temperature adsorption of copper on Au(111) was presented. The onset of copper adsorption has been shown to occur via a place-exchange mechanism at hcp sites within the Au(111)-(22 $\sqrt{3}$) reconstruction elbows. The copper-rich islands grow via an Ostwald ripening process and their top layers reconstruct in a herringbone-like fashion, albeit more disordered. The appearance of a further copper-rich layer occurs before completion of the previous one. The second layer exhibits a moiré pattern, which

remains visible for a few copper layers. The multilayer regime is characterized by the formation of pillars of pure copper. Upon annealing, copper is seen to dissolve into the bulk gold. When a few copper layers (ca. 3–4) are deposited, controlled annealing can lead to the formation of the CuAu I ($L1_0$) ordered surface alloy. The CuAu II phase may also be prepared starting from copper multilayers and annealing. Rationalization of the preparation procedures is expected to result in the production of the other ordered surface alloys. Although it appears evident that intermixing between the two metals occurs already from the onset of copper deposition, the determination of the composition of the top layer remains challenging. In particular, because of interdiffusion phenomena and the difference in reactivity of the two metals, the determination of the composition via physical or electronic methods has to be preferred to chemical titration, in order to avoid chemically induced surface segregation phenomena.

As on such prepared ordered surface alloys the sites active for molecular adsorption/desorption may be morphologically rather different and composition dependent, the study of reactions occurring over ordered surface alloys is expected to lead to a greater understanding of the underlying chemistry. On the other hand, the binding geometry and reactivity of several adsorbates can be tuned by doping the Au(111) surface with copper atoms, opening up the possibility to construct novel architectures with specific properties.

ACKNOWLEDGMENTS

The Engineering and Physical Sciences Research Council (EPSRC) is acknowledged for the funding of FG (EP/M029077/1) and RM (EP/506631/1). FG also acknowledges the European Union for funding the SURMOF project under which part of this work was undertaken (contract number NMP4-CT-2006-032109). Prof. Manfred Buck, Dr. Renald Schaub and Dr. Herbert A Früchtl are thanked for fruitful discussions and suggestions. Rodrigo M Ortiz de la Morena is acknowledged for the production of the graphical abstract. The research data supporting this publication can be accessed at http://dx.doi.org/10.17630/91713978-909d-467f-8d12-2aaa0ec320ed.

[1] F. Grillo, H. Früchtl, S. M. Francis, and N. V. Richardson, New J. Phys. **13**, 013044 (2011).
[2] T.-M. Chang and E. A. Carter, J. Phys. Chem. **99**, 7637 (1995).
[3] S.-H. Wei, A. A. Mbaye, L. G. Ferreira, and A. Zunger, Phys. Rev. B **36**, 4163 (1987).
[4] Ch. Wöll, S. Chiang, R. J. Wilson, and P. H. Lippel, Phys. Rev. B. **39**, 7988 (1989).
[5] J. A. Meyer, I. D. Baikie, E. Kopatzki, and R. J. Behm, Surf. Sci. **365**, L647 (1996).
[6] T. Lin, X. S. Shang, J. Adisoejoso, P. N. Liu, and N. Lin, J. Am. Chem. Soc. **135**, 3576 (2013).
[7] J. Liu, T. Lin, Z. Shi, F. Xia, L. Dong, P. N. Liu, and N. Lin, J. Am. Chem. Soc. **133**, 18760 (2011).
[8] F. Grillo, H. Früchtl, S. M. Francis, V. Mugnaini, M. Oliveros, J. Veciana, and N. V. Richardson, Nanoscale **4**, 6718 (2012).
[9] R. T. Seljamäe-Green, G. J. Simpson, F. Grillo, J. Greenwood, S. M. Francis, R. Schaub, J. E. Gano, H. A. Früchtl, P. Lacovig, and C. J. Baddeley, Langmuir **31**, 262 (2015).
[10] A. G. Trant, T. E. Jones, and C. J. Baddeley, J. Phys. Chem. C **111**, 10534 (2007).
[11] K. E. Wilson and C. J. Baddeley, Surf. Sci. **629**, 102 (2014).
[12] W. G. Cullen and P. N. First, Surf. Sci. **420**, 53 (1999).
[13] B. Voigtländer, G. Meyer, and N. M. Amer, Surf. Sci. **255**, L529 (1991).
[14] A. Delga, J. Lagoute, V. Repain, C. Chacon, Y. Girard, M. Marathe, S. Narasimhan, and S. Rousset, Phys. Rev. B **84**, 035416 (2011).
[15] A. E. Anderson, F. Grillo, C. R. Larrea, R. T. Seljamäe-Green, H. A. Früchtl, and C. J. Baddeley, J. Phys. Chem. C **120**, 1049 (2016).
[16] A. Rai, J. Nayak, and S. R. Barman, e-J. Surf. Sci. Nanotech. **12**, 49 (2014).
[17] I. Horcas, R. Fernández, J. M. Gómez-Rodríguez, J. Colchero, J. Gomez-Herrero, and A. M. Baró. Rev. Sci. Instrum. **78**, 013705 (2007).
[18] H. Shi, W. Wang, Z. Li, L. Wang, and X. Shao, Chinese J. Chem. Phys. **30**, 443 (2017).
[19] J. F. Jia, Y. Hasegawa, K. Inoue, W. S. Yang, and T. Sakurai, Appl. Phys. A **66** (Suppl. 1), 1125 (1998).
[20] V. De Renzi, R. Rousseau, D. Marchetto, R. Biagi, S. Scandolo, and U. del Pennino, Phys. Rev. Lett. **95**, 046804 (2005).
[21] T. K. Sham, A. Hiraya, and M. Watanabe, Phys. Rev. B **55**, 7585 (1997).
[22] T. K. Sham, M. L. Perlman, and R. E. Watson, Phys. Rev. B **19**, 539 (1979).
[23] M. Kuhn and T. K. Sham, Phys. Rev. B. **49**, 1647 (1994).
[24] J. Knudsen, A. U. Nileka, R. T. Vang, J. Schndat, E. L. Kunkes, J. A. Dumesic, M. Mavrikakis, and F. Besenbacher, J. Am. Chem. Soc. **129**, 6485 (2007).
[25] F. Besenbacher, I. Chorkendorff, B. S. Clausen, B. Hammer, A. M. Molenbroek, J. K. Nørskov, and I. Stensgaard, Science **279**, 1913 (1998).
[26] B. G. Baker, B. B. Johnson, and G. L. C. Maire, Surf. Sci. **24**, 572 (1971).
[27] H. Lei, Q. Hou, and M. Hou, Nucl. Instrum. Methods Phys. Res. B **164-165** , 537 (2000).
[28] Y. Nakai, M. S. Zei, D. M. Kolb, and G. Lehmpfuhl, Ber. Bunsenges. Phys. Chem. **88**, 340 (1984).
[29] E. J. Macur and R. W. Vook, Thin Solid Films **66**, 371 (1980).
[30] H. Lei and Y-J Tang, J. Phys.: Condens. Matter **16**, 7823 (2004).
[31] T. Trimble, L. Tang, N. Vasiljevic, N. Dimitrov, M. van Schilfgaarde, C. Friesen, C. V. Thompson, S. C. Seel, J. A. Floro, and K. Sieradzki, Phys. Rev. Lett. **95**, 166106 (2005).
[32] L. Wang, P. Li, H. Shi, Z. Li, K. Wu, and X. Shao, J. Phys. Chem. C **121**, 7977 (2017).
[33] O. M. Magnussen and R. J. Behm, J. Electroanal. Chem. **467**, 258 (1999).
[34] F. Xiang, C. Li, Z. Wang, X. Liu, D. Jiang, X. Leng, J. Ling, and L. Wang, Surf. Sci. **633**, 46 (2015).
[35] W. Wallauer and Th. Fauster, Surf. Sci. **331-333** , 731 (1995).

[36] G. Mettela and G. U. Kulkarni, CrystEngComm **17**, 9459 (2015).
[37] X. Zhao, P. Liu, J. Hrbek, J. A. Rodriguez, and M. Pérez, Surf. Sci. **592**, 25 (2005).
[38] X. Zhao and J. Rodriguez, Surf. Sci. **600**, 2113 (2006).
[39] D. D. Chambliss and S. Chiang, Surf. Sci. **264**, L187 (1992).
[40] M. B. Hugenschmidt, M. Ruff, A. Hitzke, and R. J. Behm, Surf. Sci. **388**, L1100 (1997).
[41] J. L. Stevens and R. Q. Hwang, Phys. Rev. Lett. **74**, 2078 (1995).
[42] M. Ø. Pedersen, S. Helveg, A. Ruban, I. Stensgaard, E. Lagsgaard, J. K. Norskov, and F. Besenbacher, Surf. Sci. **426**, 395 (1999).
[43] L. G. Dias, A. A. Leitão, C. A. Achete, R.-P. Blum, H. Niehus, and R. B. Capaz, Surf. Sci. **601**, 5540 (2007).
[44] C. S. Casari, S. Foglio, F. Siviero, A. Li Bassi, M. Passoni, and C. E. Bottani, Phys. Rev. B **79**, 195402 (2009).
[45] M. E. Blecher, E. A. Lewis, A. Pronschinske, C. J. Murphy, M. F. G. Mattera, M. L. Liriano, and E. C. H. Sykes, Surf. Sci. **646**, 1 (2016).
[46] V. Ozoliņš, C. Wolverton, and A. Zunger, Phys. Rev. B **57**, 6427 (1998).
[47] J. M. Howe, A. R. S. Gautam, K. Chatterjee, and F. Phillipp, Acta Mater. **55**, 2159 (2007).
[48] J. Hennig, D. Mari, and R. Schaller, Phys. Rev. B **79**, 144116 (2009).
[49] Y. Feutelaisa, B. Legendrea, and M. Guymontb, Acta Mater. **47**, 2539 (1999).
[50] A. R. S Gautam and J. M. Howe, J. Mater. Sci. **44**, 601 (2009).
[51] W. B. Pearson, *Handbook of Lattice Spacings and Structures of Metals and Alloys* (Pergamon Press, London, 1958).
[52] A. M. Silva, C. A. Achete, and R. B. Capaz, Chem. Phys. **410**, 99 (2013).
[53] L. Piccolo, A. Piednoir, and J.-C. Bertolini, Surf. Sci. **592**, 169 (2005).
[54] D. Maspoch, N. Domingo, D. Ruiz-Molina, K. Wurst, G. Vaughan, J. Tejada, C. Rovira, and J. Veciana, Angew. Chem. Int. Ed. **43**, 1828 (2004).
[55] W. Gao, T. A. Baker, L. Zhou, D. S. Pinnaduwage, E. Kaxiras, and C. M. Friend, J. Am. Chem. Soc. **130**, 3560 (2008).
[56] F. Grillo, V. Mugnaini, M. Oliveros, S. M. Francis, D. J. Choi, M. V. Rastei, L. Limot, C. Cepek, M. Pedio, S. T. Bromley, N. V. Richardson, J. P. Bucher, and J. Veciana, J. Phys. Chem. Lett. **3**, 1559 (2012).
[57] V. Mugnaini, A. Calzolari, R. Ovsyannikov, A. Vollmer, M. Gonidec, I. Alcon, J. Veciana, and M. Pedio, J. Phys. Chem. Lett. **6**, 2101 (2015).
[58] F. Silly, A. Q. Shaw, M. R. Castell, G. D. A. Briggs, M. Mura, N. Martsinovich, and L. Kantorovich, J. Phys. Chem. C **112**, 11476 (2008).
[59] Y.-P. Lin, O. Ourdjini, L. Giovanelli, S. Clair, T. Faury, Y. Ksari, J.-M. Themlin, L. Porte, and M. Abel, J. Phys. Chem. C **117**, 9895 (2013).
[60] M. M. Antonijevic and M. B. Petrovic, Int. J. Electrochem. Sci. **3**, 1 (2008).
[61] M. Finšgar, and I. Milošev, Corros. Sci. **52**, 2737 (2010).
[62] M. B. P. Mihajlović, and M. M. Antonijević, Int. J. Electrochem. Sci. **10**, 1027 (2015).
[63] F. Grillo, J. A. Garrido Torres, M.-J. Treanor, C. R. Larrea, J. P. Götze, P. Lacovig, H. A. Früchtl, R. Schaub, and N. V. Richardson, Nanoscale **8**, 9167 (2016).
[64] F. Grillo, D. W. Tee, S. M. Francis, H. Früchtl, and N. V. Richardson, Nanoscale **5**, 5269 (2013).
[65] F. Grillo, D. W. Tee, S. M. Francis, H. A. Früchtl, and N. V. Richardson, J. Phys. Chem. C **118**, 8667 (2014).
[66] K. Cho, J. Kishimoto, T. Hashizume, and T. Sakurai, Jpn. J. Appl. Phys. **33**, L125 (1994).
[67] J. Edmonson, *et al.*, in preparation.
[68] F. Grillo, *et al.*, in preparation.
[69] M. Okada, Y. Tsuda, K. Oka, K. Kojima, W. A. Diño, A. Yoshigoe, and H. Kasai, Sci. Rep. **6**, 31101 (2016).
[70] C. L. Bracey, P. R. Ellis, and G. J. Hutchings, Chem. Soc. Rev. **38**, 2231 (2009).
[71] G. Guisbiers, S. Mejia-Rosales, S. Khanal, F. Ruiz-Zepeda, R. L. Whetten, and M. José-Yacaman, Nano Lett. **14**, 6718 (2014).
[72] J. Yin, S. Shan, L. Yang, D. Mott, O. Malis, V. Petkov, F. Cai, M. S. Ng, J. Luo, B. H. Chen, M. Engelhard, and C.-J. Zhong, Chem. Mater. **24**, 4662 (2012).
[73] M. S. Li, X. D. Wang, N. Perret, and M. A. Keane, Catal. Commun. **46**, 187 (2014).
[74] M. S. Li, X. D. Wang, F. Cárdenas-Lizana, and M. A. Keane, Catal. Today **279**, 19 (2017).
[75] F. Cárdenas-Lizana, S. Gómez-Quero, C. J. Baddeley, and M. A. Keane, Appl. Catal. A **387**, 155 (2010).
[76] F. Cárdenas-Lizana, S. Gómez-Quero, A. Hugon, L. Delannoy, C. Louis, and M. A. Keane, J. Catal. **262**, 235 (2009).
[77] M. S. Li, Y. F. Hao, F. Cárdenas-Lizana, H. H. P. Yiu, and M. A. Keane, Top. Catal. **58**, 149 (2015).